coatings

MDPI

Article

ZnO Nano-Flowers Assembled on Carbon Fiber Textile for High-Performance Supercapacitor's Electrode

Qasim Abbas [1], Muhammad Sufyan Javed [2,3,*], Awais Ahmad [4], Sajid Hussain Siyal [5,*], Idress Asim [6], Rafeal Luque [4,*], Munirah D. Albaqami [7] and Ammar Mohamed Tighezza [7]

1 Department of Intelligent Manufacturing, Yibin University, Yibin 644000, China; qsandhu@yibinu.edu.cn
2 School of Physical Science and Technology, Lanzhou University, Lanzhou 730000, China
3 Department of Physics, COMSATS University Islamabad, Lahore Campus, Islamabad 54000, Pakistan
4 Departamento de Quimica Organica, Universidad de Cordoba, Edificio Marie Curie (C-3), Ctra Nnal IV-A, Km 396, E14014 Cordoba, Spain; awaisahmed@gcuf.edu.pk
5 Metallurgy & Materials Engineering Department, Dawood University of Engineering and Technology, Karachi 74800, Pakistan
6 Key Laboratory of Materials Modification by Laser, Electron, and Ion-Beams, Dalian University of Technology, Dalian 116024, China; asim.idrees44@gmail.com
7 Department of Chemistry, College of Science, King Saud University, Riyadh 11451, Saudi Arabia; muneerad@ksu.edu.sa (M.D.A.); ammar@ksu.edu.sa (A.M.T.)
* Correspondence: safisabri@gmail.com (M.S.J.); sajid.hussain@duet.edu.pk (S.H.S.); q62alsor@uco.es (R.L.)

Abstract: Herein, a crystalline nano-flowers structured zinc oxide (ZnO) was directly grown on carbon fiber textile (CFT) substrate via a simple hydrothermal process and fabricated with a binder-free electrode (denoted as ZnO@CFT) for supercapacitor (SC) utilization. The ZnO@CFT electrode revealed a 201 $F \cdot g^{-1}$ specific capacitance at 1 $A \cdot g^{-1}$ with admirable stability of >90% maintained after 3000 cycles at 10 $A \cdot g^{-1}$. These impressive findings are responsible for the exceedingly open channels for well-organized and efficient diffusion of effective electrolytic conduction via ZnO and CFT. Consequently, accurate and consistent structural and morphological manufacturing engineering is well regarded when increasing electrode materials' effective surface area and intrinsic electrical conduction capability. The crystalline structure of ZnO nano-flowers could pave the way for low-cost supercapacitors.

Keywords: ZnO; nanoflowers; carbon-fiber-cloth; electrode; supercapacitors

Citation: Abbas, Q.; Javed, M.S.; Ahmad, A.; Siyal, S.H.; Asim, I.; Luque, R.; Albaqami, M.D.; Tighezza, A.M. ZnO Nano-Flowers Assembled on Carbon Fiber Textile for High-Performance Supercapacitor's Electrode. *Coatings* **2021**, *11*, 1337. https://doi.org/10.3390/coatings11111337

Academic Editor: Emerson Coy

Received: 3 October 2021
Accepted: 25 October 2021
Published: 30 October 2021

1. Introduction

Recently, significant efforts have been made to develop electrochemically efficient-energy storing and converting devices such as batteries, supercapacitors (SCs), and fuel cells [1]. SCs have piqued the curiosity of the scientific community owing to their high energy density, better and longer cyclic life, commercial repairs, and the fact that they a higher energy density than conventional capacitors. The conductivity of the electrode material affects the performance of the SCs [2,3]. As a result, numerous nano-sized oxides are used to introduce a variety of SC electrodes containing more active sites, thereby increasing the electrode's electronic and ionic conductivity [4,5]. A number of studies have shown that transition metal oxides, such as RuO_2 [6,7], MnO_2 [8], Fe_3O_4 [9], and ZnO [10], in their respective oxidation states have been studied extensively for SC applications. Furthermore, these oxides have been demonstrated to self-assemble in a variety of nano-structured morphological features such as nanowires, nanosheets, nanorods, etc. The nanocomposite materials also considered as good for SCs such as Mn@Fe [11] and carbon coated metal oxides due to the hybrid properties of different materials [12,13]. Electrodes with all these morphological features may have considerably enhanced electrocatalytic activity for SCs due to fairly short diffusion paths, faster charge carrier transfer, and a greater number of electroactive sites [14,15].

Zn-based electrodes have been the subject of several studies as possible SC electrode material [16,17]. ZnO has the shortest energy band-gap of 3.37 eV and has recently attracted a lot of attention for its low cost and moderate electrochemical properties. For example, Chen et al. evidenced that nanorods of ZnO with MnO_2 coating had a good capacitance of 222 $F{\cdot}g^{-1}$ at 25 $mV{\cdot}s^{-1}$ with excellent cycling stability > 97.5% after 1200 cycles [18]. Gao et al. had testified that nanosheets of ZnO with graphene coating revealed a low 62.2 $F{\cdot}g^{-1}$ specific capacitance at 0.5 $A{\cdot}g^{-1}$; after 200 cycles, the capacitance decreased by only 5.1%, demonstrating good cycling stability [19]. Another study found that nanocomposites of ZnO/graphene which were synthesized had a 146 $F{\cdot}g^{-1}$ specific capacitance at 100 $mV{\cdot}s^{-1}$, showing long-term recycling performance [20]. Zhang et al. reported a greater 323.9 $F{\cdot}g^{-1}$ specific capacitance at 50 $mV{\cdot}s^{-1}$ for carbon nanotube-ZnO nanocomposites electrodes and showed that they exhibited good cyclic stability (83%) after 100 cycles [21]. Jayalakshmi et al. recounted a 21.7 $F{\cdot}g^{-1}$ specific capacitance at 50 $mV{\cdot}s^{-1}$ with better cyclic stability (of almost 100%) after 500 cycles for a composite containing ZnO and carbon [22]. It is evident that each of the aforementioned works was primarily concerned with ZnO-based composite materials for the electrode of SCs. However, since less importance is given to using ZnO as a pristine electrode material, there seems to be a deficiency in studies of ZnO applications for SCs. He et al. revealed that the ZnO-nanocones structure found by chemical fabrication exhibited 378.5 $F{\cdot}g^{-1}$ at 20 $mV{\cdot}s^{-1}$ with a cyclic stability of 65% completing 500 cycles and ZnO nanowires exhibited a capacitance of 191.5 $F{\cdot}g^{-1}$ at 20 $mV{\cdot}s^{-1}$ [23]. In another study, ZnO particles exhibited good specific capacitances prepared hydrothermally with nitrate (5.87 $F{\cdot}g^{-1}$), acetate (5.35 $F{\cdot}g^{-1}$), and chloride (4.14 $F{\cdot}g^{-1}$) specific capacitance at a 5 $mV{\cdot}s^{-1}$. Moreover, the electrodes' cyclic performances were tested for only 200 cycles [24]. According to the above findings, despite the fact that nanocomposites with zinc and ZnO pristine had also been observed to have similar capacitance values with other metal oxides although they are not very competitive [20,25]. Binders as well as additives could really assist in increasing the mechanical qualities of the SCs while also increasing electron and electrolyte ion resistance and lowering the device's power capability in commercial applications [26]. In another scenario, binder-free based electrodes could considerably improve conductivity and efficient ion diffusion routes while increasing electrode flexibility. Using a quick, easy, and cheap hydrothermal method, the electro-active electrodes can be directly grown with a range of electrically conductive bases such as nickel-foam, carbon steel foil, and carbon fabric [27–29]. Due to its superior conductivity, non-toxicity, and mechanical strength, carbon fiber textiles (CFT) are a particularly ideal base for direct creation of metallic oxide nano-structures for built-up SCs.

As a result, the growth of ZnO nano-structured via simple methods for the preparation is the key solution to these problems. To achieve this goal, nanostructures such as nano-wires, nano-rods, and nano-tubes could be directly grown on CFT or nickel-foam. Compared to powder electrodes coated using a standard liquid pasting technique, conductive surface-based electrodes offer good electrical interactions, assisting in the achievement of high electro-catalytic activity [30,31].

Herein, we reported the facile synthesis of ZnO-flower electrodes on CFT without the use of a binder which is suitable for use in solid-state SCs. Growing ZnO-flower on CFT with a post-annealing solvo-thermal procedure and a binder-free electrode is described in this paper as an easy but effective method. These qualities (such as having a low heating rate, and being cheap, fast, and easy) characterize the hydrothermal method. Studies on the ZnO-flower electrode's electrochemical properties revealed a high excellent specific capacitance of 201 $F{\cdot}g^{-1}$ at a current density of 1 and high stability of >90% capacitance maintained after 3000 cycles at 10 $A{\cdot}g^{-1}$. Growing ZnO-flower-structured using the method described in this paper could pave the way for low-cost SC electrodes that are free of the binder.

2. Experimental

2.1. The Preparation of ZnO Nano-Flowers on Carbon Fabric Cloth for a Binder-Free Electrode

All chemicals used for this work were bought from reputed chemicals suppliers named "Aladdin Chemicals suppliers and manufacturers", Shanghai, China. The carbon textile fiber (CFT), having a thickness of 0.2 mm with 1.8 g·cm^{-3} density, was purchased from a company known as "Shanghai Lishuo Composite Material Technology", Shanghai, China. The nano-flowers were directly grown on a carbon fiber textile (CFT) using the standard hydrothermal method. First, a solution mixture of 2 mmol of $Zn(CH_3CO_2)_2$, 4 mmol of NaOH, 2 mmol of cetrimonium bromide (CTAB) in 40 mL of deionized water. The prepared solution was then placed in an ultrasonicator for one hour to achieve a completely homogeneous mixture. Following that, this homogeneous ultrasonicated solution was then poured into a Teflon autoclave and filled to almost 70% capacity subsequently. A neat and clean CFT piece was put on the wall of the Teflon autoclave. The autoclave was perfectly sealed airtightly and placed inside an electronic oven at 100 °C for 10 h to initiate a simple hydrothermal process. After the hydrothermal process was completed, the CFT collected along with the ZnO ancestor was carefully washed several times with ethanol and deionized water and denoted as ZnO@CFT. The obtained ZnO@CFT material was ultra-sonicate continuously for 5 min to eliminate the remaining particles pated at the surface of CFT. The ZnO@CFT was then placed in a furnace set to 90 °C for complete dehydration. In conclusion, dehydrated ZnO@CFT was carbonized for 2 h at 350 °C to increase crystallinity. The experiment was repeated two times, and comparable results were achieved. The schematic representation of the fabrication of ZnO nano-flowers was given in Figure 1.

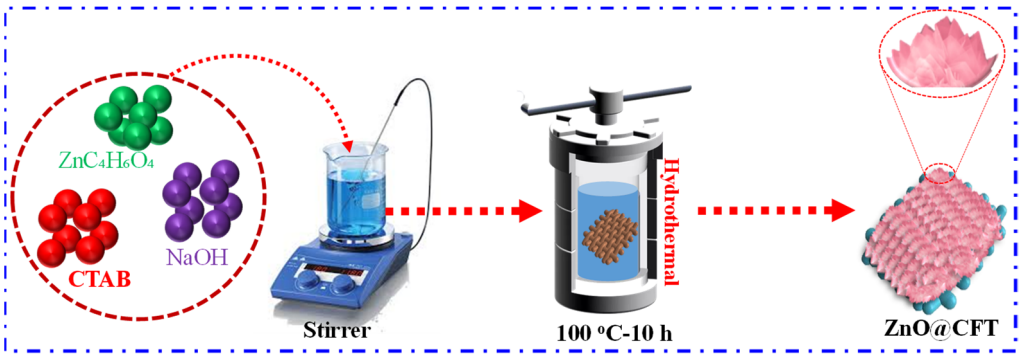

Figure 1. A schematic diagram shows the synthesis process used to develop ZnO nano-flowers directly on the surface of CFT.

2.2. ZnO@CFT Electrode Fabrication

The synthesized ZnO@CFT was cut into 1 × 1 cm^2 small pieces to use as a freestanding electrode in 1 M electrolyte of KOH for evaluating the electrochemical activity as an electrode in SCs. The active mass loading density of prepared ZnO@CFT for electrodes had been 1.26 mg·cm^2, calculated meticulously using only the mass difference between pristine CFT and annealed ZnO@CFT.

2.3. Materials Characterization

An as-prepared ZnO@CFT morphology study utilizes field emission scanning electron microscopy (FEI Nova 400). When it came to XRD powder crystal composition, the PAN-analytical X–pert diffractometer used Cu–K radiation to characterize the ZnO@CFT samples thoroughly. In order to carry out X-ray photoelectron spectroscopy (XPS), an X-ray source (Escalab (250Xi)) Al Ka (1486.5 eV) was utilized.

2.4. Measurements of Electrochemistry

The supercapacitive activity of the as-prepared ZnO@CFT electrode was evaluated using GCD (galvanostatic charge-discharge), CV (cyclic voltammetry), and EIS characterization (electrochemical impedance spectroscopy). The three-electrode configurations (for reference, Ag/AgCl, platinum sheet, and ZnO@CFT were used as reference, counter, and working electrode at room temperature) were verified in a 1M (mol·L^{-1}) KOH electrolyte using an electrochemical workstation (CHI660E, Chen Hua, Shanghai, China). Using Equation (1), the specific capacitance (C) of ZnO@CFT inside the three-electrode configuration was determined by calculating [27,30].

$$C = I\Delta t/mv \quad (1)$$

wherein C, I, m, and t represent specific capacitance (C·g^{-1}), discharge current (A), effective mass (g) of the as-prepared material, and discharge time (s), respectively.

3. Results and Discussion

Figure 1 illustrates a primary hydrothermal method used to directly develop the nano-flowers-like ZnO@CFT structure on the conductive CFT. In the presence of NaOH, Zn atoms react with O atoms, and 2 mmol of CTAB initiate a nano-flowers growing at 100 °C. FE-SEM was used to look at the surface morphology of prepared nanoparticles of ZnO, which can be seen in Figure 2. The ZnO nanostructure was found to be uniformly distributed over the conductive CFT, which is shown in Figure 2a,b. This surface is crucial to getting good electrochemical behavior from the system. An additional benefit of ZnO nanoflowers is their better working mobility, as shown in Figure 2c by the three-dimensionally consistent toughened structural properties with ununiform void space. As can be seen in Figure 2d, this high-energy storage host has a unique morphological characteristic. Using a nano-structure made of ZnO@CFT nano-flowers, a highly porous nanostructure can be created that increases surface area while also improving the conductivity of electrons and electrolyte ions.

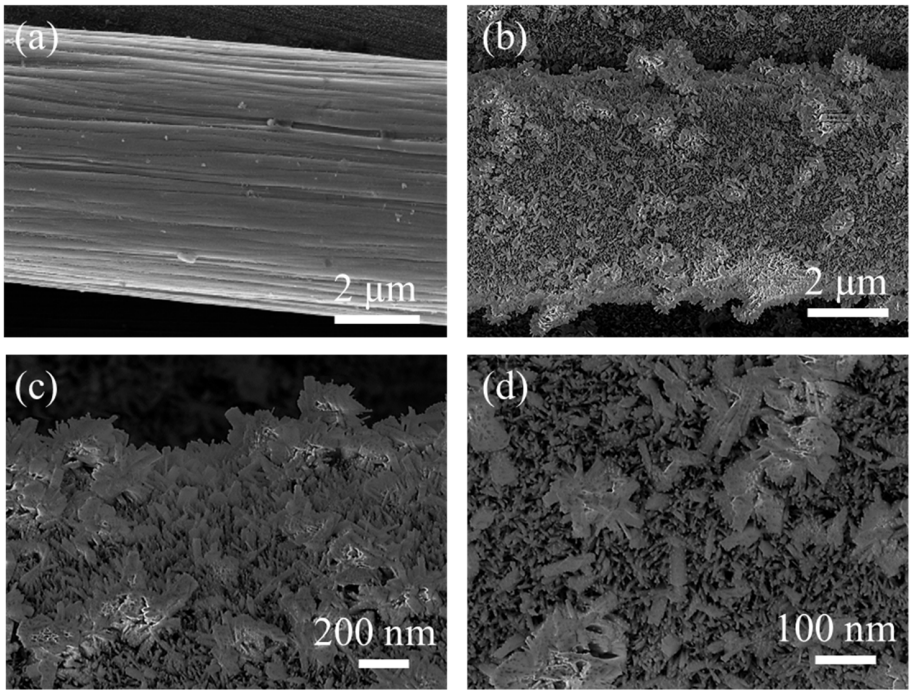

Figure 2. Morphological characteristics of ZnO@CFT electrode: (**a**) SEM image of pristine CFT and (**b**) a low-resolution FE-SEM image. (**c**) A high-resolution FE-SEM image and (**d**) a section from Figure 2c.

The XRD pattern of annealed ZnO is shown in Figure 3a, which explains its structural nature and purity. The ZnO nano-flowers diffraction peaks at 26.7°, 28.35°, 30.2°, 33.465°, 36.495°, 39.133°, 41.988°, 44.3°, 47.2°, 54.681°, 58.763°, and 62.8° could be freely indexed to the ZnO crystal planes (110), (112), (220), (222), (003), and (330), respectively. The diffraction pattern demonstrates the crystalline structure of the as-synthesized ZnO nano-flowers. There are no signs of Zn contamination, indicating that the nano-flowers are phase pure ZnO. The peak indicated with asterisk comes from CFT. Figure 3b depicts the three-dimensional crystallinity of a ZnO nano-flowers. The Zn and O atoms interconnected establish a bridge structure, which might assist quick ionic transport between the active material and the electrolyte [27,31]. ZnO is a slightly soft material with a hardness of almost 4.5 on the Mohs hardness scale. Its elastic properties are lower than those of comparable III-V semiconductor materials, such as GaN. The large specific heat, conductivity, low coefficient of thermal expansion, and high ZnO melting point are advantageous in energy storage applications.

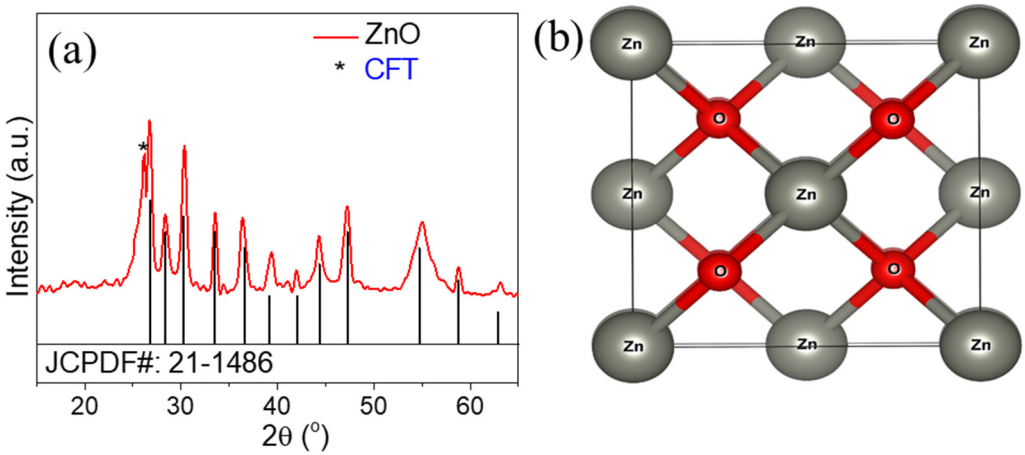

Figure 3. (**a**) XRD pattern of ZnO@CFT electrode and (**b**) crystal structure of ZnO@CF.

To better clarify these results, the oxidizing states and elemental composition of ZnO@CFT electrodes were also examined using XPS and fitted by Gaussian fitting process. The Zn 2p displayed two characteristic peaks, as shown in Figure 4a. The two diffraction peaks inside the fundamental Zn 2p spectral region at the binding affinity of 1021.6 and 1044.6 eV correlate to Zn $2p_{3/2}$ and Zn $2p_{1/2}$, respectively, with spin-orbit fracturing of 23 eV and develop a positive agreement with previous reports Zn^{2+} data [32]. The intensity peak at the least binding energy (530.8 eV) (Figure 4b) is associated with the development of metal-bonded reactive oxygen species, in which "bonded oxygen" relates to molecular oxygen formed a bond with Zn^{2+} (Zn-O) at a binding energy of 530.8 eV. The reaction kinetics redox potential is satisfied by the reduced oxygen atoms are bonded to Zn. The intensity peak (at 532.5 eV) is caused by the adsorption of loosely bonded oxygen atom "O" on the sample's surface from atmospheric humidity [33]. The XPS, as well as XRD outcomes, confirmed the ZnO nano-flowers formation on a CFT [34].

The specific surface morphology and porosity of the ZnO@CFT nano-flowers at 77 K were determined using isotherms of nitrogen adsorption-desorption. The amorphous sample takes a Brunauer–Emmett–Teller-specific surface area of approximately 89.65 $m^2 \cdot g^{-1}$. Accepting the IUPAC's classification system, the isotherms evidenced the hysteresis loop of type H1, indicating the presence of a highly porous channel [35], which can be seen in Figure 5a. The distribution of pore size, as measured by the BJH (Barrett–Joyner–Halenda) methodology from the desorption hysteresis loop, is displayed in Figure 5b. The pore size distribution of ZnO@CFT nano-flowers is largely centered at almost 6.5 nm, confirming the prepared sample's mesoporous structure. The large specific surface area improves the electrocatalytic performance and provides plenty of electro-active sites for an efficient supercapacitor [29].

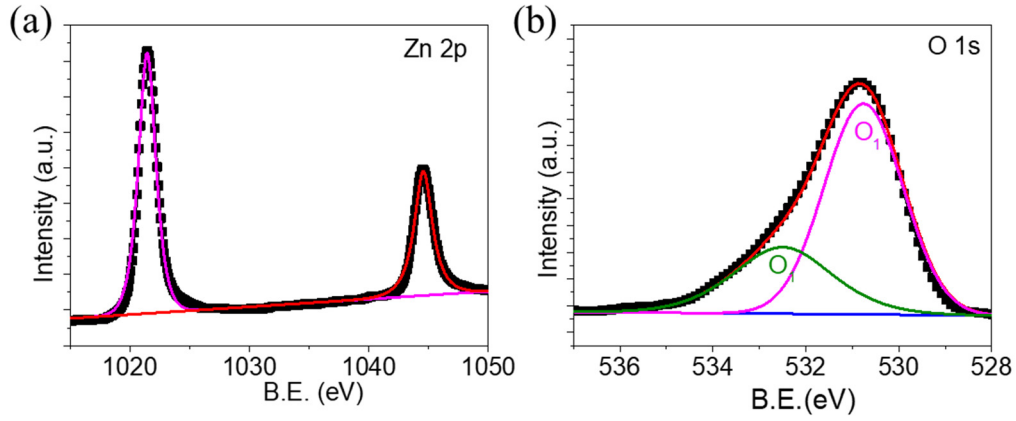

Figure 4. (**a**) Zn 2p and (**b**) O 1s core-level X-ray photoelectron spectra of ZnO nano-flowers.

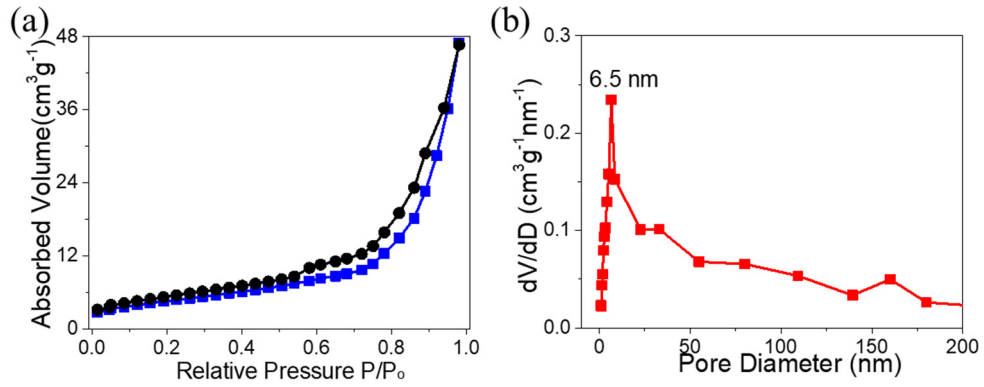

Figure 5. N_2 adsorption and desorption isotherms of ZnO nano-flowers (**a**) and pore-size distribution of ZnO nano-flowers (**b**).

The electronic properties such as CV and GCD of the ZnO@CFT electrode in the aqueous KOH electrolyte were investigated using a three-electrode cell system. Figure 6a depicts the characteristic of pristine CFT and CV curves of ZnO@CFT electrodes in a potential window of 0–0.8 V vs. Ag/AgCl at a 5 $mV \cdot s^{-1}$ scan rate. Figure 6b explains the ZnO nano-flowers electrode CV, in an aqueous KOH electrolyte, was measured at 5, 10, 20, 30, and 50 $mV \cdot s^{-1}$ scan rates in the enlarged potential window of 0 to +0.8 V vs. Ag/AgCl. Moreover, it was observed that increasing the scan rate value increases the intensity of the current, illustrating the ZnO nano-capacitance flower's behavior.

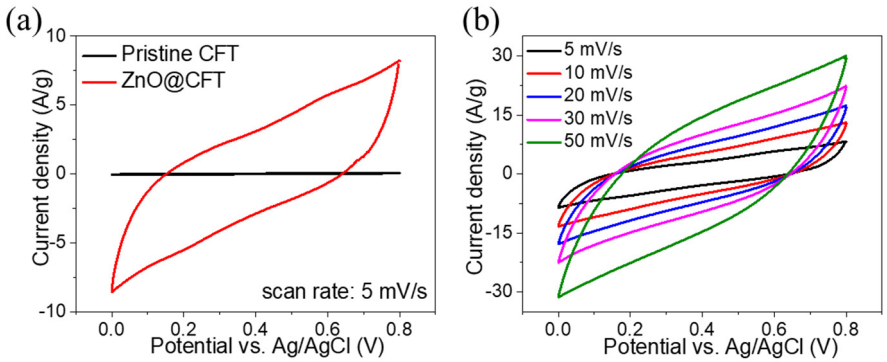

Figure 6. Electrochemical characterizations of ZnO@CFT electrode in an aqueous electrolyte of KOH: (**a**) ZnO@CFT and pristine CFT electrodes CV curves are compared (**b**) CV curves for ZnO@CFT electrodes.

The curves of GCD at current densities that vary from 1–10 A·g^{-1} were also used to verify the charging/discharging characteristic features of ZnO nano-flowers, as shown in Figure 7a. The charge/discharge curve generated an excellent capacitive performance of 201.25 F·g^{-1} at current density 1 A·g^{-1} and 125 F·g^{-1} at 10 A·g^{-1} current density. A plot of specific capacitance against current density is shown in Figure 7b. Surprisingly, at a high discharge current density of 10 A·g^{-1}, the specific capacitance of the ZnO@CFT nano-flowers electrode is reduced to 125 F·g^{-1}, resulting in a good rate performance of 62%. At all current densities, all charge/discharge curves seem to be greatly symmetric, with such a Coulombic-efficiency exceeding 90%, indicating excellent reversible efficiency and agreeing very well CV evaluation. Specific capacitance values of the ZnO@CFT (measured to use discharging curves) were 201.25, 185, 150, and 140, 125 F·g^{-1} at current densities of 1, 2, 5, 7, and 10 A·g^{-1}, respectively.

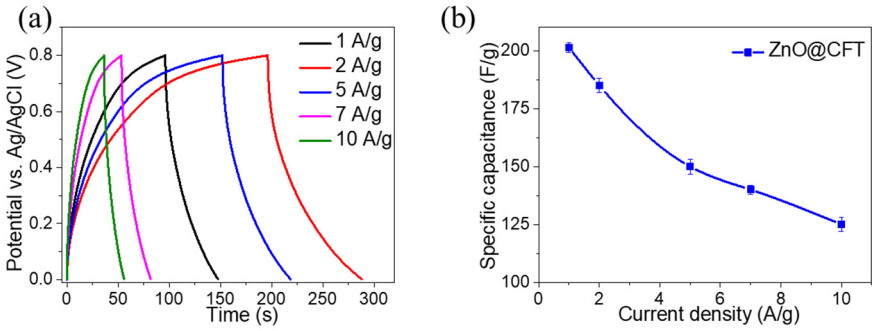

Figure 7. (**a**) Charge/discharge curves of ZnO@CFT electrodes measured against various current densities in the potential range of 0.0–0.8 V. (**b**) Specific capacitance of the ZnO@CFT electrode versus current density.

Electrochemical impedance spectroscopy (EIS) was used to investigate the electrochemical properties of the ZnO nano-flowers electrode surface. Typical Nyquist plots of ZnO@CFT nano-flowers electrodes are shown in Figure 8. Nyquist x-intercept curve represents the comparable series resistance (ESR) inside the region of high-frequency, which ultimately results from the source of impedance from multiple sources, including electrolyte, electrode material inductance, and resistance of interface [36]. The semicircle's diameter is proportional to the resistance of charge transmission on the surface of the electrode (R_{ct}) [37]. In the region of high-frequency, there is a semicircle, and in contrast, a region of low-frequency exhibited a quasi-vertical line and fitted with the electrical equivalent circuit. The inductance (Rs: 2.28 Ω) was determined by calculating the region's x-intercept of the high-frequency and the resistance of charge transmission (R_{ct}: 2.25 Ω), measured from the semicircle's diameter. The slope of the Nyquist plot keeps changing from lower to upper angles as frequency declines, exhibiting the charge-storage procedure. Additionally, EIS outcomes expose the combination of rapid electron transmission and extraordinary ion diffusion. One more key parameter for determining the possibility of Sc gadgets for industrial cases is their cycling stability.

Consequently, the cycling stability of the ZnO@CFT nano-flowers electrode was tested by deliberately running it consciously for 3000 cycles of charge/discharge at a 10 A·g^{-1} elevated current density. The cycling attitude of the ZnO@CFT electrode was investigated for 3000 cycles to determine cyclic stability, as shown in Figure 9. Excluding a relatively small (under 10%) decline throughout specific capacitance after 3000 cycles, the lengthy cycling life of ZnO@CFT reveals no discernible fade. Such cyclic stability consequences for ZnO@CFT electrodes suggested that slight variations in the physical or chemical characteristics might take place during the charge/discharge cycling method. Subsequently, the ZnO@CFT electrode retains nearly 90.32% of its initial capacity after 3000 cycles, far better than earlier reported results on the same substance and other bimetal oxides. The findings suggest that the ZnO@CFT has a remarkable capacity to keep charge

with superior stability and high efficiency during long cycling life inside the expanded potential window of 0.0–0.8 V.

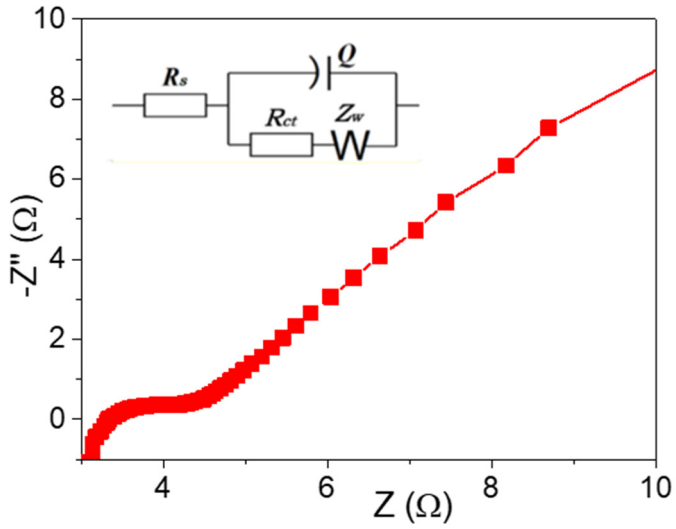

Figure 8. Nyquist plot of ZnO@CFT nano-flowers electrode.

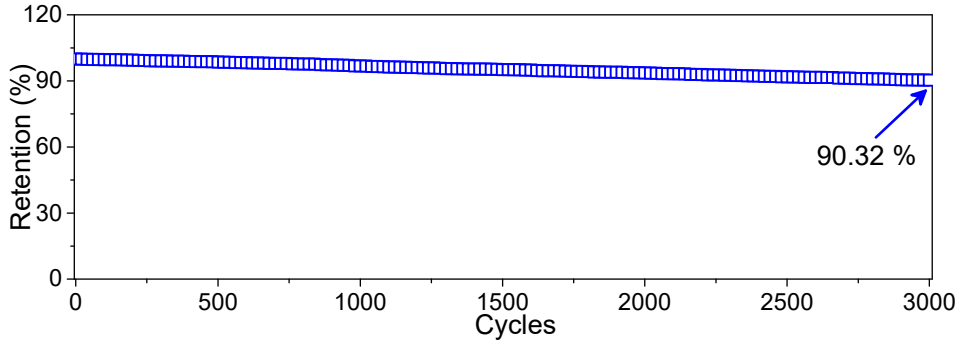

Figure 9. Capacitance retention vs. cycles number over 3000 cycles.

4. Conclusions

We designed a binder-free electrode of ZnO@CFT nano-flowers to improve the performance of SCs in the current study. A simple hydrothermal route is used to assemble ZnO nano-flowers on the surface of CFT directly. The as-prepared electrode ZnO@CFT demonstrates extraordinary electrochemical performance in a basic aqueous electrolyte, with a remarkable capacitance of 201 $F \cdot g^{-1}$ at 1 $A \cdot g^{-1}$ and the best retention at a great 10 $A \cdot g^{-1}$ current density. More fascinatingly, after 3000 charge-discharge cycles, the ZnO@CFT electrode maintains excellent stability of 90.32%. Highly open electrolyte ion and electrons transmission channels in both ZnO and CFT are responsible for such great results. The increase of the area for active surface and improvement of the electrode material's underlying conductivity, accurate morphological characteristics, and surface manufacturing engineering are well regarded.

Author Contributions: Conceptualization, M.S.J. and Q.A.; methodology, A.A.; software, S.H.S.; validation, M.S.J., I.A. and R.L.; formal analysis, M.D.A.; investigation, R.L.; resources, A.M.T.; data curation, A.M.T.; writing—original draft preparation, A.A. and M.S.J.; writing—review and editing, R.L.; visualization, S.H.S.; supervision, R.L. All authors have read and agreed to the published version of the manuscript.

Funding: This work was funded by the Researchers Supporting Project Number (RSP-2021/267) King Saud University, Riyadh, Saudi Arabia.

Institutional Review Board Statement: Not applicable.

Informed Consent Statement: Not applicable.

Data Availability Statement: Not applicable.

Conflicts of Interest: The authors declare no conflict of interest.

References

1. Shaheen, I.; Ahmad, K.S.; Zequine, C.; Gupta, R.K.; Thomas, A.G.; Malik, M.A. Green synthesis of ZnO–Co_3O_4 nanocomposite using facile foliar fuel and investigation of its electro-chemical behaviour for supercapacitors. *New J. Chem.* **2020**, *44*, 18281–18292. [CrossRef]
2. Javed, M.S.; Khan, A.J.; Ahmad, A.; Siyal, S.H.; Akram, S.; Zhao, G.; Bahajjaj, A.A.A.; Ouladsmane, M.; Alfakeer, M. Design and fabrication of bimetallic oxide nanonest-like structure/carbon cloth composite electrode for supercapacitors. *Ceram. Int.* **2021**, *47*, 30747–30755. [CrossRef]
3. Syah, R.; Ahmad, A.; Davarpanah, A.; Elveny, M.; Ramdan, D.; Albaqami, M.D.; Ouladsmane, M. Incorporation of Bi_2O_3 residuals with metallic bi as high performance electrocatalyst toward hydrogen evolution reaction. *Catalysts* **2021**, *11*, 1099. [CrossRef]
4. Siyal, S.H.; Javed, M.S.; Ahmad, A.; Sajjad, M.; Batool, S.; Khan, A.J.; Akram, S.; Alothman, A.A.; Alshgari, R.A.; Najam, T. Free-standing 3D Co3O4@NF micro-flowers composed of porous ultra-long nanowires as an advanced cathode material for supercapacitor. *Curr. Appl. Phys.* **2021**, *31*, 221–227. [CrossRef]
5. Saleem, M.; Irfan, M.; Tabassum, S.; Albaqami, M.D.; Javed, M.S.; Hussain, S.; Pervaiz, M.; Ahmad, I.; Ahmad, A.; Zuber, M. Experimental and theoretical study of highly porous lignocellulose assisted metal oxide photoelectrodes for dye-sensitized solar cells. *Arab. J. Chem.* **2021**, *14*, 102937. [CrossRef]
6. Li, H.; Li, X.; Liang, J.; Chen, Y. Hydrous RuO 2 -decorated MXene coordinating with silver nanowire inks enabling fully printed micro-supercapacitors with extraordinary volumetric performance. *Adv. Energy Mater.* **2019**, *9*, 1803987. [CrossRef]
7. Asim, S.; Javed, M.S.; Hussain, S.; Rana, M.; Iram, F.; Lv, D.; Hashim, M.; Saleem, M.; Khalid, M.; Jawaria, R.; et al. RuO2 nanorods decorated CNTs grown carbon cloth as a free standing electrode for supercapacitor and lithium ion batteries. *Electrochim. Acta* **2019**, *326*, 135009. [CrossRef]
8. Javed, M.S.; Imran, M.; Assiri, M.A.; Hussain, I.; Hussain, S.; Siyal, S.H.; Saleem, M.; Shah, S.S.A. One-step synthesis of carbon incorporated 3D MnO2 nanorods as a highly efficient electrode material for pseudocapacitors. *Mater. Lett.* **2021**, *295*, 129838. [CrossRef]
9. Khan, A.J.; Khan, A.; Javed, M.S.; Arshad, M.; Asim, S.; Khalid, M.; Siyal, S.H.; Hussain, S.; Hanif, M.; Liu, Z. Surface assembly of Fe3O4 nanodiscs embedded in reduced graphene oxide as a high-performance negative electrode for supercapacitors. *Ceram. Int.* **2020**, *46*, 19499–19505. [CrossRef]
10. Samuel, E.; Londhe, P.U.; Joshi, B.; Kim, M.-W.; Kim, K.; Swihart, M.; Chaure, N.B.; Yoon, S.S. Electrosprayed graphene decorated with ZnO nanoparticles for supercapacitors. *J. Alloy. Compd.* **2018**, *741*, 781–791. [CrossRef]
11. Laureti, S.; Peddis, D.; Del Bianco, L.; Testa, A.; Varvaro, G.; Agostinelli, E.; Binns, C.; Baker, S.; Qureshi, M.; Fiorani, D. Exchange bias and magnetothermal properties in Fe@Mn nanocomposites. *J. Magn. Magn. Mater.* **2012**, *324*, 3503–3507. [CrossRef]
12. Golubeva, E.V.; Stepanova, E.A.; Balymov, K.G.; Volchkov, S.O.; Kurlyandskaya, G.V. Magnetic properties and the giant magnetoimpedance of amorphous co-based wires with a carbon coating. *Phys. Met. Met.* **2018**, *119*, 324–331. [CrossRef]
13. Spizzo, F.; Sgarbossa, P.; Sieni, E.; Semenzato, A.; Dughiero, F.; Forzan, M.; Bertani, R.; Del Bianco, L. Synthesis of ferrofluids made of iron oxide nanoflowers: Interplay between carrier fluid and magnetic properties. *Nanomaterials* **2017**, *7*, 373. [CrossRef] [PubMed]
14. Yang, Q.; Zhang, X.T.; Zhang, M.Y.; Gao, Y.; Gao, H.; Liu, X.C.; Lui, H.; Wong, K.W.; Lau, W.M. Rationally designed hierarchical MnO2-shell/ZnO-nanowire/carbon-fabric for high-performance supercapacitor electrodes. *J. Power Sources* **2014**, *272*, 654–660. [CrossRef]
15. Cao, F.; Pan, G.; Xia, X.; Tang, P.; Chen, H. Synthesis of hierarchical porous NiO nanotube arrays for supercapacitor application. *J. Power Sources* **2014**, *264*, 161–167. [CrossRef]
16. Javed, M.S.; Lei, H.; Li, J.; Wang, Z.; Mai, W. Construction of highly dispersed mesoporous bimetallic-sulfide nanoparticles locked in N-doped graphitic carbon nanosheets for high energy density hybrid flexible pseudocapacitors. *J. Mater. Chem. A* **2019**, *7*, 17435–17445. [CrossRef]
17. Javed, M.S.; Lei, H.; Shah, H.U.; Asim, S.; Raza, R.; Mai, W. Achieving high rate and high energy density in an all-solid-state flexible asymmetric pseudocapacitor through the synergistic design of binder-free 3D $ZnCo_2O_4$ nano polyhedra and 2D layered $Ti_3C_2T_x$-MXenes. *J. Mater. Chem. A* **2019**, *7*, 24543–24556. [CrossRef]
18. Chen, H.-C.; Lyu, Y.-R.; Fang, A.; Lee, G.-J.; Karuppasamy, L.; Wu, J.J.; Lin, C.-K.; Anandan, S.; Chen, C.-Y. The design of ZnO nanorod arrays coated with MnOx for high electrochemical stability of a pseudocapacitor electrode. *Nanomaterials* **2020**, *10*, 475. [CrossRef]
19. Wang, J.; Gao, Z.; Li, Z.; Wang, B.; Yan, Y.; Liu, Q.; Mann, T.; Zhang, M.; Jiang, Z. Green synthesis of graphene nanosheets/ZnO composites and electrochemical properties. *J. Solid State Chem.* **2011**, *184*, 1421–1427. [CrossRef]
20. Lu, T.; Pan, L.; Li, H.; Zhu, G.; Lv, T.; Liu, X.; Sun, Z.; Chen, T.; Chua, D.H. Microwave-assisted synthesis of graphene–ZnO nanocomposite for electrochemical supercapacitors. *J. Alloy. Compd.* **2011**, *509*, 5488–5492. [CrossRef]

21. Zhang, Y.; Li, H.; Pan, L.; Lu, T.; Sun, Z. Capacitive behavior of graphene–ZnO composite film for supercapacitors. *J. Electroanal. Chem.* **2009**, *634*, 68–71. [CrossRef]
22. Jayalakshmi, M.; Palaniappa, M.; Balasubramanian, K. Balasubramanian, single step solution combustion synthesis of ZnO/carbon composite and its electrochemical characterization for supercapacitor application. *Int. J. Electrochem. Sci.* **2008**, *3*, 96–103.
23. He, X.; Yoo, J.E.; Lee, M.H.; Bae, J. Morphology engineering of ZnO nanostructures for high performance supercapacitors: Enhanced electrochemistry of ZnO nanocones compared to ZnO nanowires. *Nanotechnology* **2017**, *28*, 245402. [CrossRef]
24. Alver, Ü.M.İ.T.; Tanrıverdi, A.; Akgül, Ö. Hydrothermal preparation of ZnO electrodes synthesized from different pre-cursors for electrochemical supercapacitors. *Synth. Met.* **2016**, *211*, 30–34. [CrossRef]
25. Luo, Q.; Xu, P.; Qiu, Y.; Cheng, Z.; Chang, X.; Fan, H. Synthesis of ZnO tetrapods for high-performance supercapacitor applications. *Mater. Lett.* **2017**, *198*, 192–195. [CrossRef]
26. Javed, M.S.; Lei, H.; Wang, Z.; Liu, B.-T.; Cai, X.; Mai, W. 2D V2O5 nanosheets as a binder-free high-energy cathode for ultrafast aqueous and flexible Zn-ion batteries. *Nano Energy* **2020**, *70*, 104573. [CrossRef]
27. Abbas, Y.; Yun, S.; Javed, M.S.; Chen, J.; Tahir, M.F.; Wang, Z.; Yang, C.; Arshad, A.; Hussain, S. Anchoring 2D NiMoO4 nano-plates on flexible carbon cloth as a binder-free electrode for efficient energy storage devices. *Ceram. Int.* **2020**, *46*, 4470–4476. [CrossRef]
28. Li, Y.H.; Li, Q.Y.; Wang, H.Q.; Huang, Y.G.; Zhang, X.H.; Wu, Q.; Gao, H.-Q.; Yang, J.H. Synthesis and electrochemical properties of nickel–manganese oxide on MWCNTs/CFP substrate as a super-capacitor electrode. *Appl. Energy* **2015**, *153*, 78–86. [CrossRef]
29. Javed, M.S.; Chen, J.; Chen, L.; Xi, Y.; Zhang, C.; Wan, B.; Hu, C. Flexible full-solid state supercapacitors based on zinc sulfide spheres growing on carbon textile with superior charge storage. *J. Mater. Chem. A* **2016**, *4*, 667–674. [CrossRef]
30. Gogotsi, Y.; Penner, R.M. Energy Storage in Nanomaterials–Capacitive, Pseudocapacitive, or Battery-Like? ACS Publications: Washington, DC, USA, 2018.
31. Javed, M.S.; Shaheen, N.; Hussain, S.; Li, J.; Shah, S.S.A.; Abbas, Y.; Ahmad, M.A.; Raza, R.; Mai, W. An ultra-high energy density flexible asymmetric supercapacitor based on hierarchical fabric decorated with 2D bimetallic oxide nanosheets and MOF-derived porous carbon polyhedra. *J. Mater. Chem. A* **2019**, *7*, 946–957. [CrossRef]
32. Lin, J.C.; Peng, K.C.; Liao, H.L.; Lee, S.L. Transparent conducting Sc-codoped AZO film prepared from ZnO: Al–Sc by RF-DC sputtering. *Thin Solid Film.* **2008**, *516*, 5349–5354. [CrossRef]
33. Chang, F.-M.; Brahma, S.; Huang, J.-H.; Wu, Z.-Z.; Lo, K.-Y. Strong correlation between optical properties and mechanism in deficiency of normalized self-assembly ZnO nanorods. *Sci. Rep.* **2019**, *9*, 1–9. [CrossRef]
34. György, E.; del Pino, A.P.; Logofatu, C.; Duta, A.; Isac, L. Effect of nitrogen doping on wetting and photoactive properties of laser processed zinc oxide-graphene oxide nanocomposite layers. *J. Appl. Phys.* **2014**, *116*, 024906. [CrossRef]
35. Ravikovitch, P.I.; Neimark, A. Characterization of nanoporous materials from adsorption and desorption isotherms. *Colloids Surfaces A Physicochem. Eng. Asp.* **2001**, *187–188*, 11–21. [CrossRef]
36. Zhang, J.; Kong, L.-B.; Cai, J.-J.; Luo, Y.-C.; Kang, L. Nanoflake-like cobalt hydroxide/ordered mesoporous carbon composite for electrochemical capacitors. *J. Solid State Electrochem.* **2010**, *14*, 2065–2075. [CrossRef]
37. Shi, S.; Zhuang, X.; Cheng, B.; Wang, X. Solution blowing of ZnO nanoflake-encapsulated carbon nanofibers as electrodes for supercapacitors. *J. Mater. Chem. A* **2013**, *1*, 13779–13788. [CrossRef]